THE INFLUENCE OF FIBRE ANGLE ON THE COMPRESSIVE STRENGTH OF DELAMINATED SURFACE PLIES

A.T. Rhead, R. Butler* and N. Baker
Department of Mechanical Engineering, University of Bath, Bath, UK.
* Corresponding author(R.Butler@bath.ac.uk)

Keywords: *Buckling, Delamination, Propagation, Poisson's ratio*

Abstract
An extremely efficient Strip Model which predicts the applied strain below which initial local buckle-driven propagation of a delamination will not occur is applied to a $\pm\theta^o$ surface sublaminate. The Strip Model is shown to perform well, compared to experiments and Finite Element Analysis, when the mismatch between the Poisson's ratio of the full laminate and surface sublaminate is less than 0.5. Laminates with larger mismatches which induce lateral compression in the sub-laminate propagate earlier than predicted. Mismatches that put the delaminated sublaminate into transverse tension are shown to improve resistance to delamination propagation. The most favourable surface plies, both in terms of strength following delamination and buckling capacity of the full laminate are confirmed to be $\pm 45^o$.

1 Introduction

Composite laminates subject to compression following Barely Visible Impact Damage (BVID) are known to fail at loads significantly below those of pristine laminates. Often this is due to the propagation of delaminations following local sublaminate buckling. Aerospace regulations specify that composite laminates must tolerate BVID without failure typically reducing allowable strains to around 4,500 μstrain. In some applications this gives strengths that are less than 50% of the equivalent values for aluminium. Although the Compression After Impact (CAI) strength of laminates comprising of 0^o, $\pm 45^o$ and 90^o plies is reasonably well understood, other laminates employing plies with angles such as $\pm 30^o$ and $\pm 60^o$ are less well understood. Additionally, new fibre steering technologies are giving rise to laminates with the full gamut of $\pm\theta^o$ sublaminates, producing varied CAI problems and novel behaviour.

The method usually adopted for modelling propagation following local buckling is non-linear Finite Element analysis using cohesive elements or virtual crack closure techniques [1-3]. However, such methods are complex and require large computational effort and so do not lend themselves to understanding the mechanisms affecting damage tolerance. Hence, the development of simplified methods to capture such mechanisms is required in order to improve design of laminates for damage tolerance.

In earlier work [4], the authors extended the principles of Strain Energy Release Rate (SERR) considered by others [5-7] for one-dimensional propagation of an isotropic strut containing a delamination to the case of a two-dimensional, anisotropic plate. In this paper, new extensions to the extremely efficient Strip Model recently derived in [1] are used to model propagation of a near surface-delamination. Uniaxial compression tests are reported for laminates with an artificial delamination creating a $\pm\theta^o$ sublaminate. Previously unseen effects related to mismatches in Poisson's ratio (ν) between the base and sublaminates were noted in these experiments and are investigated herein.

2. The Strip Model

As described in [4] and extended in [1] the Strip Model predicts critical threshold values of applied strain below which local buckle-driven propagation of a delamination will not occur. The modelling is comprised of two parts, the first is the calculation of the local buckling strain ε^C using the infinite strip program VICONOPT [8]. Following conventional design principles which seek to avoid undesirable coupling effects the overall laminate is assumed to be balanced and symmetric. A thin-film assumption is made which enforces zero curvature in the parent laminate. Hence the loads acting on the sublaminate

Table 1. Experimental and analytical local buckling strains and threshold propagation strains for laminates with a range of laminate and sublaminate Poisson's ratios. In all cases an artificial delamination of diameter 39mm is placed at the 2nd ply interface.

Stacking sequence	ν_L	$\nu_{\pm\theta}$	$\nu_{\pm\theta} - \nu_L$	ε^c (μstrain)			ε_{th} (μstrain)		
				Exp.	Strip Model	FEA [3]	Exp.	Strip Model	FEA [3]
$[0_2/\pm45/90/\pm45/90]_S$	0.32	0.35	0.03	1250*	676	619	3540	3552	3583
$[\pm30/0/90_2/0/90/0]_S$	0.20	1.43	1.23	1400	444	-	3600	4804	-
$[\pm30/0_2/\pm30/30/\mp60/\pm30/30/0_2/\mp30]$	0.85	1.43	0.58	1731	622	-	4127	4698	-
$[\pm45/0_2/-45/90/+45/90]_S$	0.32	0.79	0.47	3010*	793	687	6700	6567	7350
$[\pm60/0_2/\pm30/\mp30]_S$	0.64	0.32	-0.32	-	90900	-	-	90970	-
$[90_2/\pm45/0/\mp45/0]s$	0.32	0.02	-0.30	-	7092	-	-	7647	-

*Delayed experimental buckling due to adhesion.

$\{N\}_{SL}$ are determined by obtaining the strain $\{\varepsilon\}_L$ of the full parent laminate when unit axial strain is applied. $\{N\}_{SL}$ is then calculated, by assuming compatibility of strain from,

$$\begin{Bmatrix} N_x \\ N_y \\ N_{xy} \end{Bmatrix}_{SL} = \begin{bmatrix} A_{11} & A_{12} & A_{13} \\ A_{12} & A_{22} & A_{23} \\ A_{13} & A_{23} & A_{33} \end{bmatrix}_{SL} \begin{Bmatrix} \varepsilon_x \\ \varepsilon_y \\ \gamma_{xy} \end{Bmatrix}_L \quad (1)$$

where $[A]_{SL}$ is the in-plane membrane stiffness matrix of the sublaminate. These loads are applied to the sublaminate during VICONOPT analysis to calculate the sublaminate buckling strain ε^C. The second stage [1] is the calculation of the propagation strain ε_{th}. An equivalent Mode I approximation of the actual, mixed-mode SERR is established by assuming simplified components of bending and membrane (strain) energy in the post-buckled, thin sub-laminate created by the delamination. A comparison of bending and membrane energies in the sublaminate prior to and following propagation is then used to calculate the compressive threshold strain ε_{th} for the sublaminate, resulting in the equation,

$$\varepsilon_{th} = \varepsilon^C \left(\sqrt{4 + \frac{2G_{1C}}{A_{nn}(\varepsilon^C)^2}} - 1 \right) \quad (2)$$

where $A_{nn,SL}$ is the axial stiffness of the sub-laminate and $n = 1$ when $A_{11} > A_{22}$ or $n = 2$ when $A_{22} > A_{11}$. G_{IC} is the strain energy release rate required to cause Mode I fracture in the matrix material.

3. Experimental Set-up

Table 1 gives stacking sequences for six laminates (with 0°, ±30°, ±45°, ±60° and 90° plies outermost) manufactured from 0.25mm thick Hexcel T700GC/M21 pre-preg CFRP layers with material properties E_{11} = 136 GPa, E_{22} = 8.9 GPa, G_{12} = 4.5 GPa, ν_{12} = 0.35 and G_{1C} = 550 J/m^2. In order to produce an artificial delamination each laminate had a single non-stick circle of polytetrafluoro-ethylene (PTFE) 0.0125mm thick and 39mm diameter introduced during manufacture. In each case the delamination was placed at the second ply interface, on one side only. The test coupons will subsequently be referred to using the sub-laminate stacking sequence (or in the case of the ±30° laminates, the full laminate sequence).

In order for axial compression tests to take place laminates were fitted into a compression rig, see [1], consisting of two end fixtures producing fully clamped conditions and a circular anti-buckling guide of internal diameter 85mm, see Fig. 1. Prior to compression, laminates were loaded until local buckling occurred to ensure no adhesion remained between the PTFE and the laminate. During the experiments axial compression was applied in the x direction (see Fig.1) under displacement control at 0.1 mm/min until local delamination propagation occurred or, in cases where local buckling did not occur, until laminates suffered global failure. Buckling modes and failure sequences were monitored using a Digital Image Correlation (DIC)

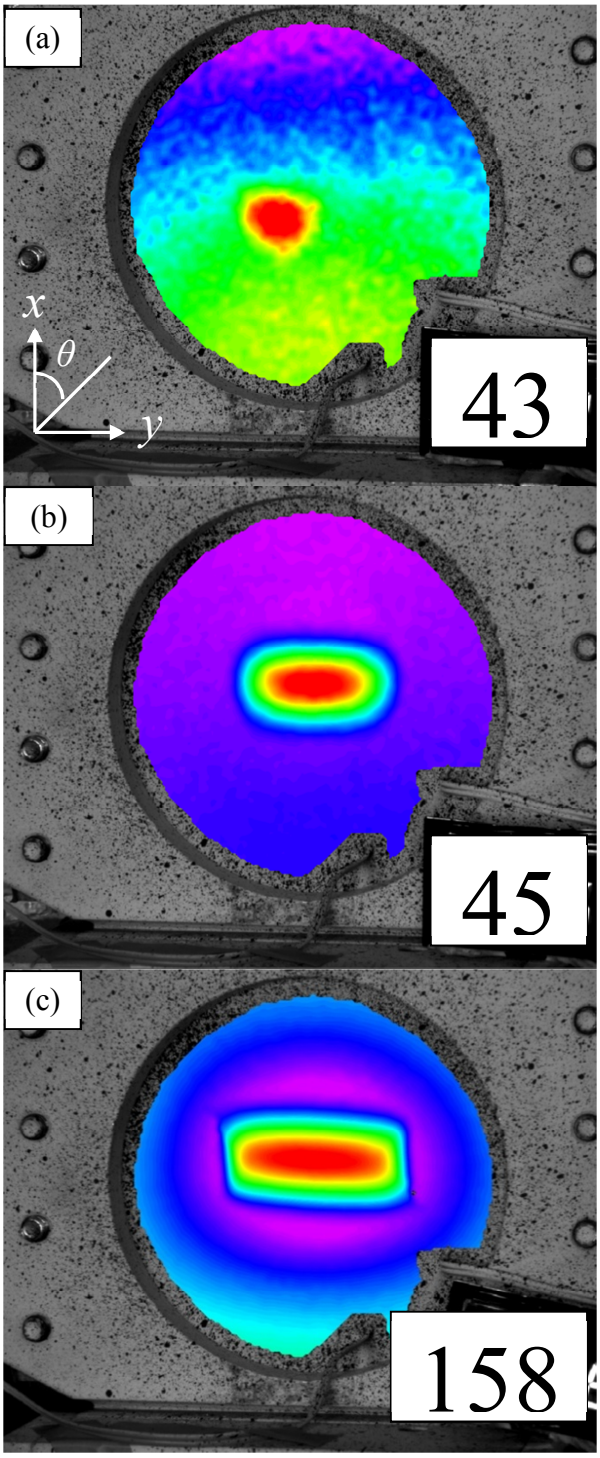

Fig. 1. DIC images of $[\pm 30/0/90_2/0/90/0]_S$ of Table 1 showing (a) initial local buckling, (b) local buckling following snap and (c) propagated state with local/global buckling interaction. Ply angle θ is shown in (a) and numbers indicate axial load in kN.

system which employs a pair of stereo cameras to measure 3D surface displacement. To ensure specimens were correctly aligned and placed under pure axial compression, strains were recorded throughout the tests by two pairs of vertically aligned back-to-back strain gauges, see Fig. 1.

4. Results

Table 1 gives buckling and threshold strain results for the coupons described in Section 3. The reported experimental strains are an average based on the four strain gauges correlated with buckling and propagation events observed using the DIC system. (Additional results for artificially delaminated layups with 2 and 3 ply thick sublaminates can be found in [1] and [9].) Both $\pm 30^o$ laminates failed as a result of sublaminate buckling leading to delamination propagation, e.g. see Fig. 1. The $\pm 60^o$ coupon did not display any local buckling but instead failed as a result of edge stresses induced by large differences in ply angle at the 2nd interface (see Fig. 2). For an explanation of this mechanism see [10]. The 90_2^9 laminate did not display any local bucking but instead failed locally through thickness near the clamped end of the coupon following global buckling of the laminate.

Fig. 2. Post failure image of the $\pm 60^o$ laminate showing evidence of edge failure.

5. Discussion

As shown in Table 1 and seen previously in [1], the Strip Model predicts delamination propagation strains for laminates with 0_2^9 and $\pm 45^o$ sublaminates to within 2% of experimental values; a better correlation than with FEA.

Unlike 0_2^9 and $\pm 45^o$ sublaminates, laminates with $\pm 60^o$ and $\pm 30^o$ sublaminates are heavily influenced by Poisson's ratio mismatches between the sub and full laminates. Figure 3 uses the Strip Model to explore the effect on damage tolerance of mismatches between the full laminate Poisson's ratio (ν_L) and the sublaminate Poisson's ratio ($\nu_{\pm\theta}$).

Plotted against the left hand ε_{th} axis of Fig. 3 are Strip Model results for $\pm\theta$ sublaminates at four values of ν_L. Note that the influence of the laminate Poisson's ratio ν_L is defined in eqn. (1) by setting

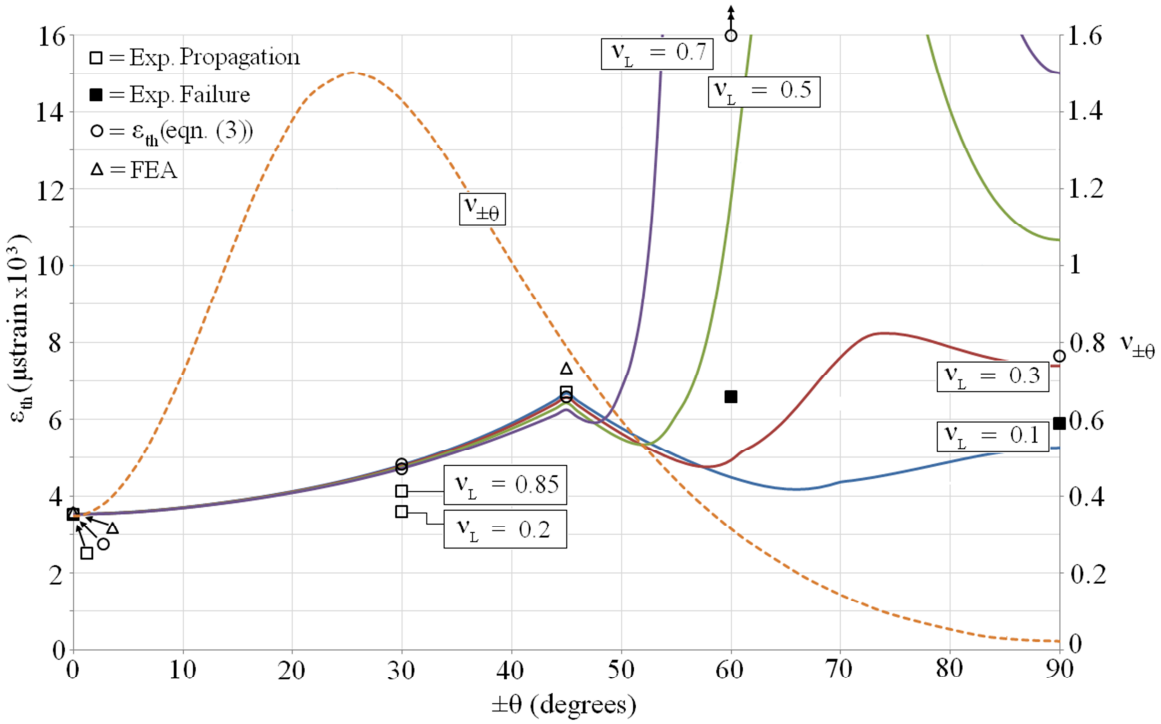

Fig. 3. Strip Model delamination propagation ε_{th} results (solid lines) for all $\pm\theta^o$ sublaminates at four values of laminate Poisson's ratio ν_L identifying outer ply angles beneficial for damage tolerance. Overlaid are Poisson's ratio values $\nu_{\pm\theta}$ (dotted line) for $\pm\theta^o$ sublaminates. Experimental, Strip Model and FEA results are represented by squares, circles and triangles, respectively. Squares are open when failure occurred via delamination propagation (following sublaminate buckling) and closed for other modes of failure.

$\varepsilon_y = -\nu_L\varepsilon_x$. This assumes $N_y = N_{xy} = 0$ (i.e. uniaxial compression) in the full laminate. Thus all laminates can be classified based on the sublaminate stacking sequence and ν_L see [11]. The dashed curve plotted against the right hand axis is the $\nu_{\pm\theta}$ of the $\pm\theta^o$ sublaminates calculated using T700GC/M21 material properties in the equation,

$$\nu_{\pm\theta} = \left(\frac{A_{12}}{A_{22}}\right)_{SL} \qquad (3)$$

For sublaminates with $0 < \pm\theta^o < 45$, ν_L has little influence on the ε_{th} curves of Fig. 3. This is because the only effect ν_L has on ε_{th} is to alter ε^C and for this range of $\pm\theta^o$ eqn. (2) is dominated by sublaminate stiffness A_{11}. This can be seen by considering $\varepsilon^C \to 0$ in eqn. (2) or alternatively by analysing Fig. 4. Figure 4 shows that ε^C remains low for $0^o \leq \pm\theta \leq 40^o$ which is a consequence of Poisson's ratio mismatches causing induced transverse compression (i.e. $\nu_{\pm\theta} > \nu_L$) for all $\pm\theta > 10^o$. When $\nu_L > \nu_{\pm\theta}$ transverse tension is induced in the sublaminate which acts to delay buckling and as shown on the right hand side of Fig. 4 as the ratio of ν_L to $\nu_{\pm\theta}$ increases $\varepsilon^C \to \infty$, which implies ε^C terms dominate eqn. (2). Kinks seen in the ε^C curves in Fig. 4 such as those between points **b** and **c** and **c** and **d** are a consequence of the change in the number of half-waves in the modeshape predicted by VICONOPT as shown on the insets of Fig. 4. Experimental coupon results together with the corresponding Strip Model results and, where available, FEA results from [1] are plotted on Fig. 3.

As can be seen from Figs. 3 and 4, the significant mismatch in the low $\nu_{\pm\theta}$ and high ν_L (see Table 1) for the $\pm60^o$ laminate means the Strip Model predicts an ε^C which far exceeds the experimental failure strain for this laminate (see Table 1 and Fig. 3). This clearly demonstrates that the laminate will not fail as a result of local buckle-driven delamination propagation. This was borne out in the experimental tests as seen in Fig. 2 which shows a symmetric delamination failure about the core of central plies which is independent of the artificial delamination.

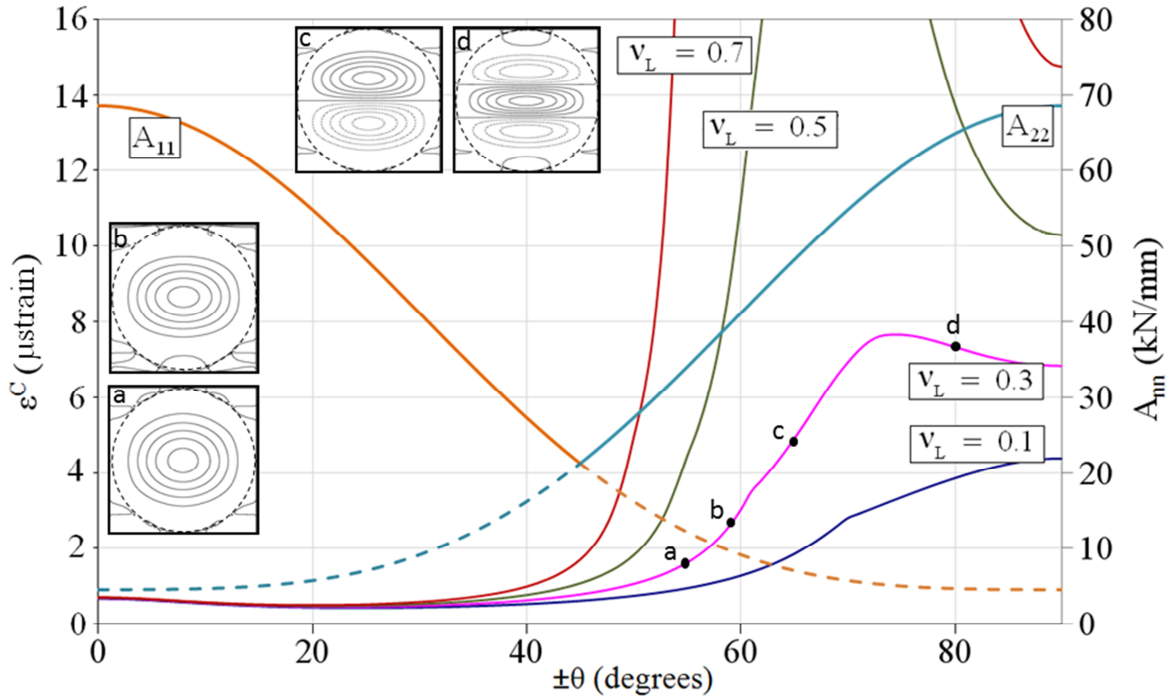

Fig. 4. VICONOPT predictions of sublaminate buckling strain at four values of laminate Poisson's ratio ν_L corresponding to those in Fig. 3. Overlaid are A_{11} and A_{22} values for $\pm\theta^o$ sublaminates with dashed lines indicating when the A_{nn} value is not used in eqn. (3). Inset are contour plots of VICONOPT buckling modes, in which load is applied vertically, corresponding to points **a**, **b**, **c** and **d**.

Thus it is believed that the $\pm 60^o$ laminate failed as a result of edge effects [10].

Sublaminate, snap-through buckling from an initially asymmetric modeshape into a symmetric modeshape (contrast Figs. 1 (a) and (b)) was observed in both $\pm 30^o$ laminates. The initial local buckle and subsequent mode jump occurred at strains significantly higher than those predicted by VICONOPT, see Table 1 and Fig. 3. This effect may be due to a skewed stress distribution in the buckled region as a result of the extension twist coupling terms B_{13} and B_{23} which are non-zero for all $\pm\theta^o$ sublaminates, with B_{13} peaking at approximately $\pm 30^o$. This creates an M_{xy} twisting moment which due to the twisting enforced contact between the base and sublaminate may resist initial buckling. It is envisaged that the twisting response may have been initiated by the small out-of-plane imperfection caused by the PTFE insert. This conclusion is supported by the asymmetric nature of the initial local buckle and subsequent asymmetric delamination growth (see Fig. 1(c)).

In the delamination propagation phase the high $\nu_{\pm\theta}$ of the $\pm 30^o$ laminates and the associated induced transverse compression gives rise to additional inter-ply stresses, which may have caused the experimental coupons to fail at strains below that predicted by the Strip Model which does not take these effects into account. The effects are especially acute in the post-buckling phase where $\nu_{\pm\theta}$ is additionally affected by the curvature caused by the interaction of the local buckle with a global laminate buckle (see Fig. 1(b)) which violates the thin film assumption of the strip model. As shown by the difference in experimental results for the $\pm 30^o$ laminates in Table 1, this effect becomes even more pronounced, for the $[\pm 30/0/90_2/0/90/0]_S$ laminate which has a low ν_L and thus a large Poisson's ratio mismatch inducing high inter-ply stresses. In addition the B_{13} and B_{23} induced M_{xy} is amplified by a relatively small ν_L leading to non-linear post-buckling behaviour which is likely to have had an impact on the experimental ε_{th} as shown in Table 1.

The above implies the use of $\pm 30^o$ plies on the surface of a laminate should be avoided where possible, particularly in cases where ν_L is low. Although this is easily accomplished in conventional laminate stacking sequence selection where ply

angle variation across interfaces can be easily controlled, it may become a problem for tow steered laminates which have a variable range of near surface $\pm\theta^o$ pairs.

Figure 3 demonstrates that delamination propagation following local buckling can be delayed by (depending on the full laminate ν) placing ±45 to $\pm 70^o$ plies on the outside of the laminate.

In closing, it is important to consider the stiffness requirement of the full laminate. A study using ESDU sheet 80023 [12] was conducted to investigate the buckling load of a simply supported square plate under uniaxial compression for $\pm\theta^o$ surface sublaminates affixed symmetrically to a generic low stiffness isotropic core. Results showed that the peak buckling load occurred with $\pm 45^o$ sublaminates and steadily reduced as the sublaminate angle increased to $\pm 70^o$. This indicates that a balance must be struck between designing panels for damage tolerance and buckling resistance.

6. Conclusions and Future Work

The Strip Model is shown to perform well, compared to experiments and Finite Element Analysis, when the mismatch between the Poisson's ratio of the full laminate and surface sublaminate is less than 0.5. Further work is required to adapt the Strip Model for cases where the delaminated sublaminate has a high Poisson's ratio and/or strong in-plane/out-of-plane coupling response such as is the case with a $\pm 30^o$ surface sublaminate.

Poisson's ratio mismatches between the full laminate and sublaminate can have beneficial effects, such as is in the case of a $\pm 60^o$ sublaminate where transverse tensile stresses can be induced, delaying local buckling of the delaminated sublaminate. However, care should be exercised as such laminates may be far from optimal for plate buckling.

Angles between 0^o and $\pm 30^o$ should be avoided as outer plies. In the case of the former this is due to the increased load that is drawn into the sublaminate and for the latter is a result of the very high Poisson's ratio of the sublaminate, which introduces compressive interply stresses that can lead to early delamination propagation. The most favourable surface plies, both in terms of strength following delamination and buckling capacity of the full laminate, are confirmed to be $\pm 45^o$.

References

[1] R. Butler, A.T. Rhead, W. Liu and N. Kontis "Compressive strength of delaminated aerospace composites". *Phil. Trans. Roy. Soc. Part A* (under review).

[2] A. Riccio, F. Caramuzzino and P. Perugini. "Embedded delamination growth in composite panels under compressive load". *Composites: Part B*, Vol.32, pp.209-218, 2001.

[3] F. Shen, K.H. Lee and T.E. Tay "Modeling delamination growth in laminated composites". *Comp. Sci. Tech,* Vol.61, pp.1239-1251, 2001.

[4] A.T. Rhead and R. Butler "Compressive static strength model for impact damaged laminates". *Compos. Sci. Technol*. Vol.69, No.14, pp.2301-2307, 2009.

[5] H. Chai, C.D. Babcock and W.G. Knauss "One dimensional modelling of failure in laminated plates by delamination buckling". *Int. J. Structures*, Vol.17, No.11, pp.1069-1083, 1981.

[6] J.W. Hutchinson and Z. Suo "Mixed mode cracking in layered materials". *Adv. Appl. Mech.*, Vol. 29, pp 63-191, 1992.

[7] J.G. Williams "On the calculation of energy release rates for cracked laminates". *Int. J. Frac.*, Vol. 36, pp 101-119, 1992.

[8] F.W. Williams, D. Kennedy, R. Butler and M.S. Anderson "VICONOPT: program for exact vibration and buckling analysis or design of prismatic plate assemblies" *AIAA J.* Vol. 29, pp.1927–1928, 1991.

[9] A. T. Rhead and R. Butler "Buckling, propagation and stability of delaminated anisotropic layers" Proceedings of ECCM 14, Budapest, Hungary, 2010.

[10] M.T. Fenske and A. J. Vizzini "The inclusion of in-plane stresses in delamination criteria". *J. Comp. Mats.*, Vol.35, No.15, pp. 1325-1342, 2001.

[11] N. Baker and R.Butler "Compression after impact modeling of damage tolerant composite laminates". Proceedings of the 51st AIAA/ASME/ASCE/ AHS/ASC Structures, Structural Dynamics, and Materials Conference, Orlando FL, AIAA-2010-2868, 2010.

[12] ESDU 80023, "Buckling of rectangular specially orthotropic plates". www.esdu.com.